

EFFECT OF STIFFNESS MATRICES TERMS ON DELAMINATION FRONT SHAPE IN LAMINATES WITH ELASTIC COUPLINGS

Jakub Rzeczkowski ^{a,*}, Sylwester Samborski ^a, Paolo S. Valvo ^b

^a *Department of Mechanical Engineering, Lublin University of Technology, Nadbystrzycka 36, 20-618 Lublin, Poland*

^b *Department of Civil and Industrial Engineering, University of Pisa, Largo Lucio Lazzarino, I-56122 Pisa, Italy*

Abstract

Analytical and fractographic analysis were led on carbon fiber reinforced plastic (CFRP) laminates subjected to double cantilever beam (DCB) test. Specimens with delamination interfaces $\theta//-\theta$, $\theta//\theta$ and $0^\circ//\theta$ were investigated. Analysis was conducted according to classical laminate theory (CLT) toward the behavior of laminate and possible presence of elastic couplings. Components of matrices **A**, **B** and **D**, as well as the parameters D_c and B_t were obtained using the Matlab software environment. Fractographic analysis was performed after the DCB tests in order to evaluate the shape of delamination front in specimens with different interfaces. The results showed that couplings between the bending moment and twisting curvature, as well as between the twisting moment and mid-plane normal strains, were strongly dependent on specimen plies orientation at delamination plane. The phenomena of elastic couplings caused non-uniform delamination front which may produce inaccuracies in fracture toughness determination. Moreover, an additional analysis of the influence of θ layers on the B_{16} and the D_{16} terms responsible for the mid-plane shear deformation and the twisting curvature was performed. The results indicated that greater number of the same layers significantly amplifies undesirable effects of elastic couplings.

1. Introduction

Fiber-reinforced polymeric (FRP) laminates have a wide array of applications in contemporary structures, such as primary and secondary load-carrying components of aircrafts and vehicles. Such advanced composite laminates demonstrate excellent potential for reducing not only structural self-weight, but also lifetime maintenance costs thanks to their high corrosion and fatigue resistance [1]. Unfortunately, composite laminates are also susceptible to a number of damage phenomena, in particular delamination, which may significantly reduce their mechanical properties and ultimately lead to structural failure [2].

The double cantilever beam (DCB) test is currently standardized for the measurement of the mode I interlaminar fracture toughness, or critical energy release rate, G_{IC} , of composite laminates [3]. Besides, international standards also cover the measurement of the mode II interlaminar fracture toughness, G_{IIC} , based on the end-notched flexure (ENF) [4] and end loaded split (ELS) tests [5]. Further testing methods have been defined to analyze mode III and mixed-mode fracture conditions [6]. Yet, it should be noted that, strictly speaking, the above-mentioned standard testing methods apply only to unidirectional (UD) laminates with mid-plane delaminations, *i.e.* laminates with stacking sequence $[0^\circ/0^\circ/.../0^\circ//0^\circ/0^\circ/.../0^\circ] = [0^\circ_n//0^\circ_n]$ [7]. Here and in the following, a slash (/) denotes the interface between two generic plies and a double slash (//) denotes the (initial) position of the delamination plane. When the standard testing methods are applied to multidirectional (MD) laminates, the obtained values of critical energy release rate, G_C , will depend on the particular stacking sequence, ply orientation at the delamination interface, and applied load type. Also, the mode mixity, *i.e.* the ratio between the mode I and II contributions to G_C , will depend on the cited parameters [8]. In general, the experimental values of G_C in modes II and III turn out to be higher than in mode I [9].

In literature, there is a bundle of papers concerning the effects of the stacking sequence on the G_C values in MD laminates. However, most studies are limited to the effects of ply orientation at

the delamination interface only. Pereira *et al.* [10] performed DCB tests on woven glass/epoxy MD laminates with starter delaminations at $\theta//-\theta$ and $0^\circ//\theta$ interfaces. During the tests, interply damage and crack branching to another interface were often observed after variable propagation lengths. Nevertheless, such phenomena did not prevent the measurement of valid initiation values of G_C , which were higher for the specimens with $\theta//-\theta$ delamination than for the specimens with $0^\circ//0^\circ$ delamination. In particular, initiation values of G_C for $0^\circ//\theta$ delamination specimens turned out to be θ -independent. De Moraes *et al.* [11] obtained G_C values for carbon/epoxy $[(0^\circ/90^\circ)_6/(0^\circ/90^\circ)_6]$ specimens with starter crack at the mid-plane, between 0° and 90° layers. The measured values of critical energy release rate were higher than those of unidirectional $[0^\circ_{12}/0^\circ_{12}]$ specimens, especially for the final propagation values. In this respect, it should be noted that even if the tested specimens were geometrically symmetric, *i.e.* with mid-plane delaminations, and loaded by symmetric loads, their stacking sequences (except for the UD laminates) were generally asymmetric, which induces a mode II contribution to the energy release rate. In general, DCB tests performed on asymmetric laminates should be regarded as I/II mixed-mode tests [12]. Hence, the values measured by De Moraes *et al.* [11] for the $[(0^\circ/90^\circ)_6/(0^\circ/90^\circ)_6]$ specimens correspond to a mixed-mode interlaminar fracture toughness, G_C , not to the pure mode I interlaminar fracture toughness, G_{IC} . This explains the higher values obtained with respect to the UD specimens.

Pereira *et al.* [13] also conducted ENF tests on carbon/epoxy MD laminates. The obtained G_C values (under prevailing mode II) increased with the ply angle θ for specimens with both $\theta//-\theta$ and $0^\circ//\theta$ delamination interfaces. Choi *et al.* [14] performed ELS tests on specimens with $45^\circ// -45^\circ$ delamination interfaces and obtained G_{IIC} values from 45 to 84% higher than those of UD specimens. Laksimi *et al.* [15] studied the effects of stacking sequence on the delamination

behavior of glass/epoxy MD laminates with $\theta//-\theta$ delamination interfaces subjected to DCB tests. For small angles ($\theta \leq 30^\circ$), they observed delamination crack propagation on the specimen mid-plane, while for larger angles ($\theta > 67^\circ$), they reported failure by flexure at the head of the precrack; for intermediate angles, they obtained delamination propagation in staircase.

Gong *et al.* [16] proposed a theoretically sound approach to conduct pure mode I DCB tests on MD laminates with $\theta//\theta$ and $\theta//-\theta$ delamination interfaces. In particular, to ensure material symmetry, they suitably designed the specimen stacking sequences by imposing the same extensional and bending stiffnesses – and no bending-extension coupling – to the specimen arms. They found that G_{IC} depends on the interface angle θ and its distribution of along the delamination front becomes more and more uniform as the specimen width increases.

-

To sum up, in most studies, all of the laminate elastic couplings – such as shear-extension coupling, bending-extension coupling, and bending-twisting coupling – are simply neglected or set to zero on purpose to ensure simpler testing conditions and interpretation of experimental results. Yet, coupling phenomena are intrinsic attributes of layered FRP structures with different orientations of reinforcing fibers in plies, in particular when the layups are non-symmetric.

In this paper, we present an analysis of the behavior of carbon fiber-reinforced polymer (CFRP) epoxy MD laminates with different delamination interfaces subjected to DCB tests (under prevailing mode I loading). Additionally, fractographic analysis was performed in order to evaluate delamination front after the DCB tests. Additional analytical analysis was conducted towards influence of number of θ layers on B_{16} and D_{16} components.

2. Analysis of behavior of multidirectional laminates subjected to the mode I loading

2.1 Effects of elastic coupling in DCB and ENF tests

The well-known constitutive relations of classical lamination theory (CLT) relate the in-plane force vector $\mathbf{N} = [N_x, N_y, N_{xy}]^T$ and bending moment vector $\mathbf{M} = [M_x, M_y, M_{xy}]^T$ with the in-plane strain vector $\boldsymbol{\varepsilon} = [\varepsilon_x, \varepsilon_y, \varepsilon_{xy}]^T$ and curvature vector $\boldsymbol{\kappa} = [\kappa_x, \kappa_y, \kappa_{xy}]^T$ as follows (see also Appendix A) [7]:

$$\begin{cases} N_x \\ N_y \\ N_{xy} \end{cases} = \begin{bmatrix} A_{11} & A_{12} & A_{16} \\ A_{12} & A_{22} & A_{26} \\ A_{16} & A_{26} & A_{66} \end{bmatrix} \begin{cases} \varepsilon_x \\ \varepsilon_y \\ \gamma_{xy} \end{cases} + \begin{bmatrix} B_{11} & B_{12} & B_{16} \\ B_{12} & B_{22} & B_{26} \\ B_{16} & B_{26} & B_{66} \end{bmatrix} \begin{cases} \kappa_x \\ \kappa_y \\ \kappa_{xy} \end{cases}$$

$$\begin{cases} M_x \\ M_y \\ M_{xy} \end{cases} = \begin{bmatrix} B_{11} & B_{12} & B_{16} \\ B_{12} & B_{22} & B_{26} \\ B_{16} & B_{26} & B_{66} \end{bmatrix} \begin{cases} \varepsilon_x \\ \varepsilon_y \\ \gamma_{xy} \end{cases} + \begin{bmatrix} D_{11} & D_{12} & D_{16} \\ D_{12} & D_{22} & D_{26} \\ D_{16} & D_{26} & D_{66} \end{bmatrix} \begin{cases} \kappa_x \\ \kappa_y \\ \kappa_{xy} \end{cases}$$
(1)

Equation (1) shows that the coupling behavior depends on the internal form of the extensional stiffness matrix, \mathbf{A} , bending-extension coupling matrix, \mathbf{B} , and bending stiffness matrix, \mathbf{D} . According to York [17], matrices \mathbf{A} and \mathbf{D} can only have two forms:

- uncoupled, when

$$\begin{aligned} A_{16} &= A_{26} = 0 \\ D_{16} &= D_{26} = 0 \end{aligned}$$
(2)

- coupled, when

$$\begin{aligned} A_{16} &\neq A_{26} \neq 0 \\ D_{16} &\neq D_{26} \neq 0 \end{aligned}$$
(3)

The bending-extension coupling matrix, \mathbf{B} , besides its uncoupled variant \mathbf{B}_0 , can take five different forms: \mathbf{B}_L , \mathbf{B}_T , \mathbf{B}_{LT} , \mathbf{B}_S and \mathbf{B}_F , described in detailed by York. Accordingly, up to

twenty-four types of coupled laminates are possible with thousands of possible layups. Among them, the bending-extension (BE) and bending-twisting (BT) couplings [18,19] have strong influence on the variation on the energy release rate along the crack front in DCB and ENF specimens, as previously studied by an author of this paper [20,21]. In such studies, it has been shown that the non-uniformity in the energy release rate across a specimens width can be quantified in terms of two non-dimensional parameters:

$$D_c = \frac{D_{12}^2}{D_{11}D_{22}} \quad (4)$$

$$B_t = \frac{|D_{16}|}{D_{11}} \quad (5)$$

where D_{ij} are the elements of the bending stiffness matrices of the arms of the specimen. For specially orthotropic laminates ($B_t=0$), the distribution of G is symmetric with respect to the center of the specimen with minima at the outer edges for the DCB test and maxima for the ENF test. In this case, the variation in G along the delamination front is caused by the anticlastic curvature caused by saddle-shaped deformation of the specimen arms due to longitudinal and transverse bending coupling [22]. The magnitude of D_c correlates with the G values at the edges and in the center of the specimen with straight delamination front. Since the crack position is normally monitored at the edges, D_c should be minimized to avoid significant errors in G_{IC} measurements. Hence, Davidson [23] suggested that the specimens should be designed so that D_c is less or equal 0.25, which can be obtained by relaxing the restriction of special orthotropy. This minimization leads to the appearance of bending-twisting coupling and skew G distribution. Moreover, the asymmetry of the energy release rate distribution about specimen center for initially straight delamination front as well as the asymmetry of the shape of propagating

delamination front is a function of the parameter B_t . Ideally, both D_c and B_t should be relatively small to ensure self-similar delamination growth with uniform G distribution along the crack front. This result can be obtained by manufacturing multidirectional laminates with suitable stacking sequences. The finite elements analyses conducted by de Moraes [24] proved, that the effect of mode mixity and curved delamination front in the measurements of G_I could be minimized by a proper selection of specimen stacking sequence.

2.2. Analysis of delamination front

2.2.1. Test specimens

Tests were performed on carbon/epoxy composite laminates with the following stacking sequences: $[0^\circ_{18}/\theta//-\theta/0^\circ_{18}]$, $[0^\circ_{18}/\theta//\theta/0^\circ_{18}]$, and $[0^\circ_{18}/0//\theta/0^\circ_{18}]$, where the fiber orientation angle θ was chosen in the set $\{0^\circ, 30^\circ, 45^\circ, 60^\circ, 90^\circ\}$. In order to investigate the shape of the delamination front, the DCB specimens were opened in their mid-planes after the experimental tests and observed by using an OptaTech optical microscope. Additionally, calculations according to CLT were performed to study the influence of the laminate lay-ups. All calculations were performed in the Matlab software environment assuming for the laminate the mechanical properties obtained from previous tensile tests on UD laminated specimens (see Table 1).

Table 1. Mechanical properties of carbon/exoxy UD laminate

E_1 [GPa]	E_2 [GPa]	ν_{12} [-]	G_{12} [GPa]
112.105	7.421	0.27	3.338

In the DCB test, the upper arm of the specimen is subjected to the following point-wise varying bending moment vector:

$$\begin{bmatrix} M_x \\ 0 \\ 0 \end{bmatrix} = \begin{bmatrix} B_{11} & B_{12} & B_{16} \\ B_{21} & B_{22} & B_{26} \\ B_{16} & B_{26} & B_{66} \end{bmatrix} \begin{Bmatrix} \varepsilon_x \\ \varepsilon_y \\ \gamma_{xy} \end{Bmatrix} + \begin{bmatrix} D_{11} & D_{12} & D_{16} \\ D_{21} & D_{22} & D_{26} \\ D_{16} & D_{26} & D_{66} \end{bmatrix} \begin{Bmatrix} \kappa_x \\ \kappa_y \\ \kappa_{xy} \end{Bmatrix} \quad (20)$$

2.2.2. Specimens with $\theta//-\theta$ delamination interfaces

For the antisymmetric $\theta//-\theta$ laminates, not all of the components of the **B** matrix are equal to zero. In the mid-plane of laminate the antisymmetric off-axis layers compensate each other, so that twisting deformation is not present under bending moment ($D_{16}=0$). Instead, in the coupling matrix the same antisymmetric pairs amplify each other ($B_{16} \neq 0$) and make the bending moment coupled to the shear strain. The coupling terms related to the in-plane strains compensate each other ($B_{11}=B_{12}=0$). The values of the stiffness matrix components and parameters D_c and B_t for the tested laminates with $30^\circ// -30^\circ$, $45^\circ// -45^\circ$, and $60^\circ// -60^\circ$ delamination interfaces are presented in Table 2. For laminates with interfaces $30^\circ//30^\circ$ and $60^\circ//60^\circ$ the values of the matrix components are the same, as well as the D_c parameter. For the $45^\circ// -45^\circ$ laminate, the value of D_{16} is about two times smaller, whereas D_c is greater. The B_{16} component causes the laminate to be in tension on one side and in compression on the other one, so that the crack tip is not symmetrical with respect to the specimen width as presented in Figure 1.

Table. 2. Stiffness matrices components and coupling parameters for laminates with $\theta//-\theta$ delamination interfaces.

interface	B [MPa mm ²]			D [MPa mm ³]			D_c	B_t
$30^\circ// -30^\circ$	0	0	581.6749	100.5488	31.8849	0	0.4655	0
	0	0	199.9969	31.8849	21.7220	0		
	581.6749	199.9969	0	0	0	33.8702		
$45^\circ// -45^\circ$	0	0	451.2984	51.5129	41.5074	0	0.6493	0
	0	0	451.2984	41.5074	51.5129	0		
	451.2984	451.2984	0	0	0	43.4926		
$60^\circ// -60^\circ$	0	0	581.6749	100.5488	31.8849	0	0.4655	0

	0	0	199.9969	31.8849	21.7220	0		
	581.6749	199.9969	0	0	0	33.8702		

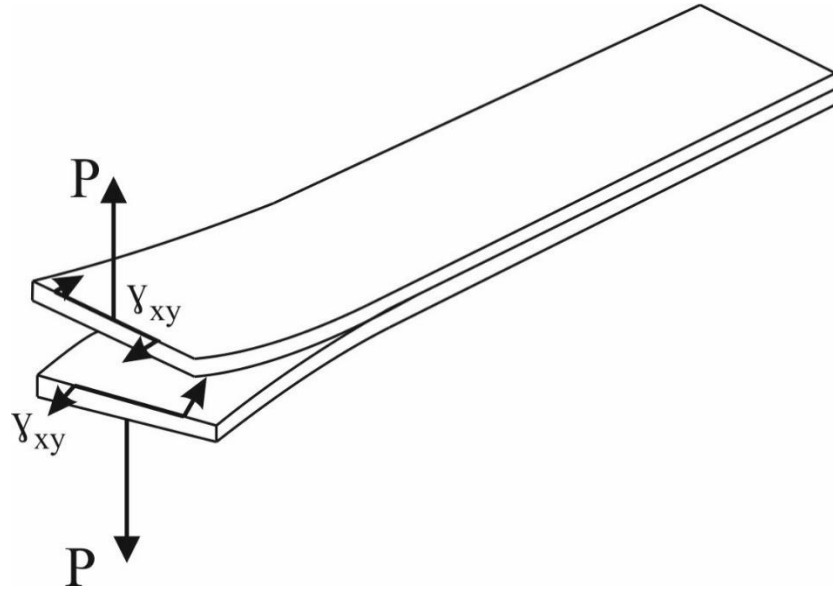


Figure 1. Influence of γ_{xy} strain on the deformation of DCB specimens with $\theta//-\theta$ delamination interfaces.

Fractographic analysis of $45^\circ// -45^\circ$ and $60^\circ// -60^\circ$ laminates after the DCB tests are shown in Figures 2 and 3. The red and blue lines respectively denote the actual delamination front and the crack tip positions observed on the specimen edges. The delamination front turns out to be irregular and with a certain degree of skewness due to the influence of the in-plane shear strain. Skewness can be inferred also from visual inspection of the crack-tip positions on the specimen edges. Exterior visual inspection is however insufficient to predict the real (non-straight) shape of the delamination front. The assumption of a regular, straight delamination front can cause inaccuracies in the determination of the critical energy release rate.

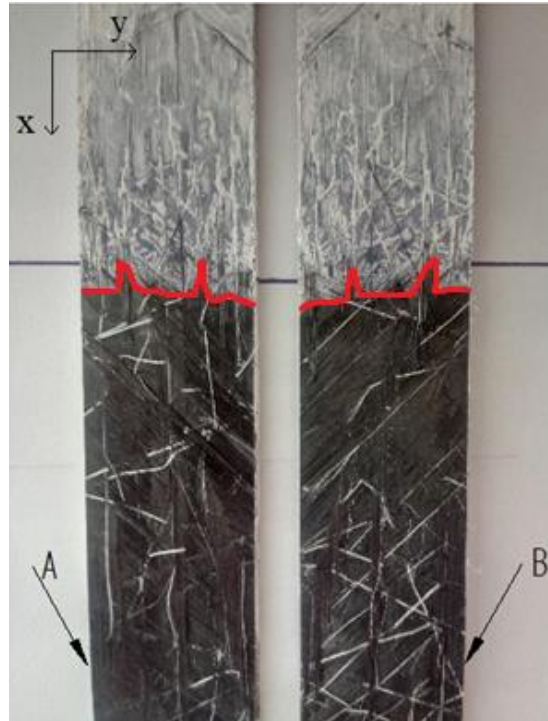


Figure 2. Delamination front in specimen with $45^\circ// -45^\circ$ delamination interface after the DCB test.

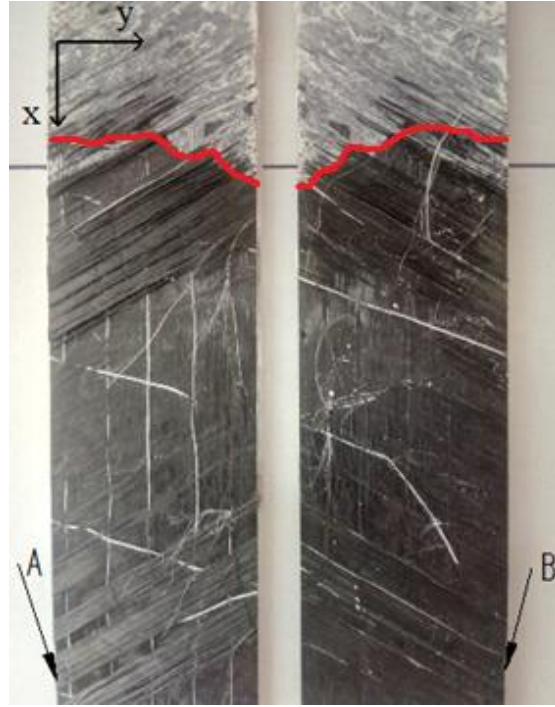


Figure 3. Delamination front in specimen with $60^\circ//\text{--}60^\circ$ delamination interface after the DCB test.

2.2.3. Specimens with $\theta//\theta$ delamination interfaces

In $\theta//\theta$ symmetric laminates, there are two identical layers with the same orientation placed symmetrically about the mid-plane. Such off-axis layers - without balancing layers in the overall stacking sequence - results in a non-zero D_{16} term, which causes twist curvature under bending load, as shown in Figure 4. All of the components of matrix **B** are equal to zero, hence the in-plane strains and shear strains do not exist under bending load. Table 3 shows the values of the components of matrices **B** and **D**, as well as of the coupling parameters D_c and B_t , for the tested laminates with $0^\circ//0^\circ$, $30^\circ//30^\circ$, $45^\circ//45^\circ$, and $60^\circ//60^\circ$ delamination interfaces. The greatest value of D_c is calculated for the laminate with the $45^\circ//45^\circ$ interface, the lowest value for the UD laminate. The value of parameter B_t increases with the angle θ . For the UD laminate, the D_{16} component is equal to zero, so that twist curvature does not exist under bending load. As a consequence, the coupling parameters are minimal.

Table. 3. Stiffness matrices components and coupling parameters for laminates with $\theta//\theta$ delamination interfaces.

interface	B [MPa mm ²]			D [MPa mm ³]			D_c	B_t
0°//0°	0	0	0	168.8296	3.0175	0	0.0048	0
	0	0	0	3.0175	11.1760	0		
	0	0	0	0	0	5.0028		
30°//30°	0	0	0	100.5488	31.8849	50.7996	0.4655	0.5052
	0	0	0	31.8849	21.7220	17.4664		
	0	0	0	50.7996	17.4664	33.8702		
45°//45°	0	0	0	51.5129	41.5074	39.4134	0.6493	0.7651
	0	0	0	41.5074	51.5129	39.4134		
	0	0	0	39.4134	39.4134	43.4926		
60°//60°	0	0	0	21.7220	31.8849	17.4664	0.4655	0.8041
	0	0	0	31.8849	100.5488	50.7996		
	0	0	0	17.4664	50.7996	33.8702		

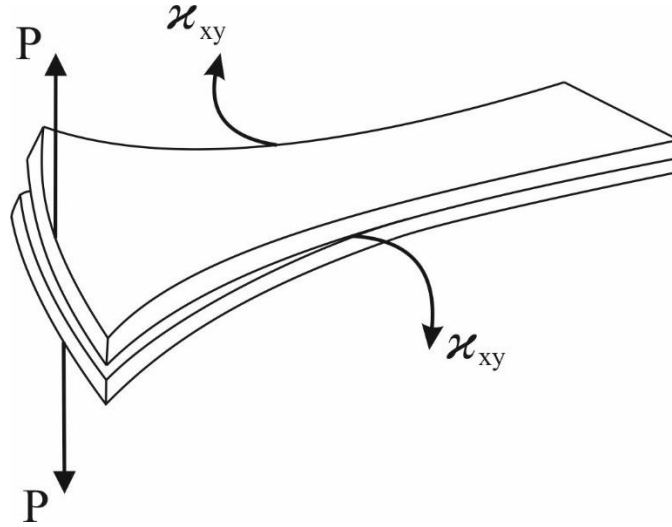


Figure 4. Influence of κ_{xy} curvature on the deformation of DCB specimens with $\theta//\theta$ delamination interfaces.

Fractographic analysis of specimens with 60°//60° delamination interfaces showed a strongly irregular delamination front (red line), as depicted in Figure 5. The real shape of the delamination front is also much different from what would be expected from mere visual inspection of the crack-tip positions (blue lines) on the specimen edges.

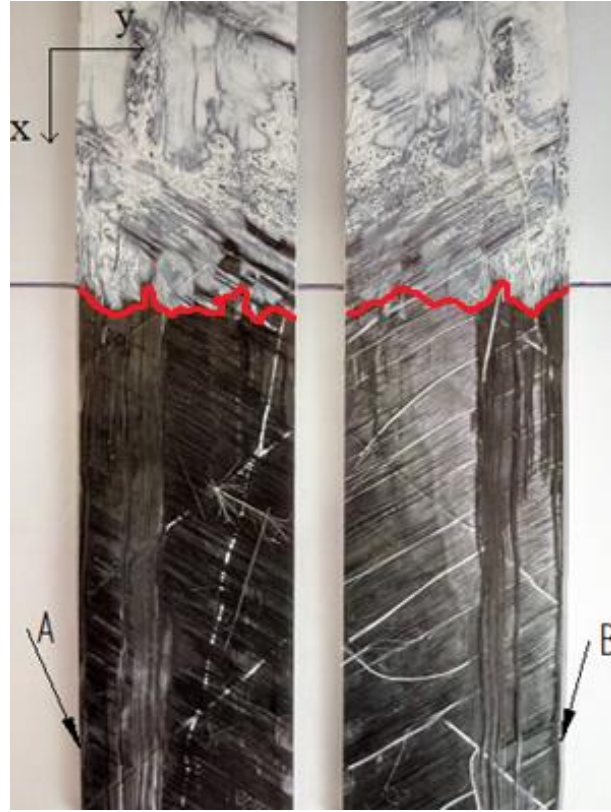


Figure 5. Delamination front in specimen with $60^\circ//60^\circ$ delamination interface after the DCB test.

2.2.4. Specimens with $0^\circ//\theta$ delamination interfaces

Laminates with $0^\circ//\theta$ delamination interfaces have non-zero terms in the **B** and the **D** matrices, which cause simultaneously twisting curvature and shear deformation under bending load, as shown in Figure 6. The specimen with $0^\circ//90^\circ$ interface is a special case of cross-ply laminate, in which all layers are oriented in the longitudinal or transverse directions. In cross-ply laminates, the abovementioned shear and twist coupling effects do not exist under bending load ($B_{16}=0$, $D_{16}=0$) and only in-plane shear deformation appears. Table 4 presents the values of the components of the stiffness matrices and coupling coefficients for the tested laminates with

$0^\circ//30^\circ$, $0^\circ//45^\circ$, $0^\circ//60^\circ$, and $0^\circ//90^\circ$ delamination interfaces. The values of the coupling parameters are all relatively small and very close to zero for the $0^\circ//90^\circ$ cross-ply laminates.

Fractographic analysis reveals that for $0^\circ//30^\circ$ specimens the delamination front is a straight skewed line with sharp breakage on one side, where for the $0^\circ//45^\circ$ specimens the delamination front is firmly non-uniform. The $0^\circ//90^\circ$ laminate exhibited a symmetric delamination front with respect to the center of the laminate. This result is compatible with the absence of couplings between bending moments and in-plane shear and twisting curvature. Delamination fronts for all of the tested $0^\circ//\theta$ specimens are presented in Figures 7, 8, and 9.

Table. 4. Stiffness matrices components and coupling parameters for laminates with $0^\circ//\theta$ delamination interfaces.

interface	B [MPa mm ²]			D [MPa mm ³]			D_c	B_t
$0^\circ//30^\circ$	-390.9206	165.2714	290.8374	134.6892	17.4512	25.3998	0.1375	0.1866
	165.2741	60.3778	99.9984	17.4512	16.4490	8.7332		
	290.8374	99.9984	165.2714	25.3998	8.7332	19.4365		
$0^\circ//45^\circ$	-671.6603	220.3619	225.6492	110.1712	22.2625	19.7067	0.1435	0.1789
	220.3619	230.9365	225.6492	22.2625	31.3444	19.7067		
	225.6492	225.6492	220.3619	19.7067	19.7067	24.2477		
$0^\circ//60^\circ$	-842.2190	165.2714	99.9984	95.2758	17.4512	8.7332	0.0572	0.0917
	165.2714	511.6762	290.8374	17.4512	55.8624	25.3998		
	99.9984	290.8374	165.2714	8.7332	25.3998	19.4365		
$0^\circ//90^\circ$	-902.5968	0	0	90.0028	3.0175	0	0.0011	6.2 e-19
	0	902.5968	0	3.0175	90.0028	0		
	0	0	0	0	0	5.0028		

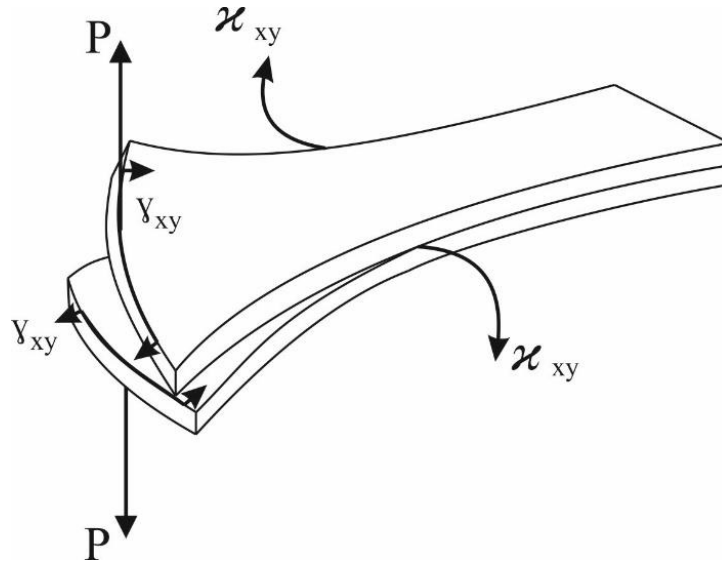


Figure 6. Influence of γ_{xy} strain and κ_{xy} curvature on the deformation of DCB specimens with $0^\circ//\theta$ delamination interfaces.

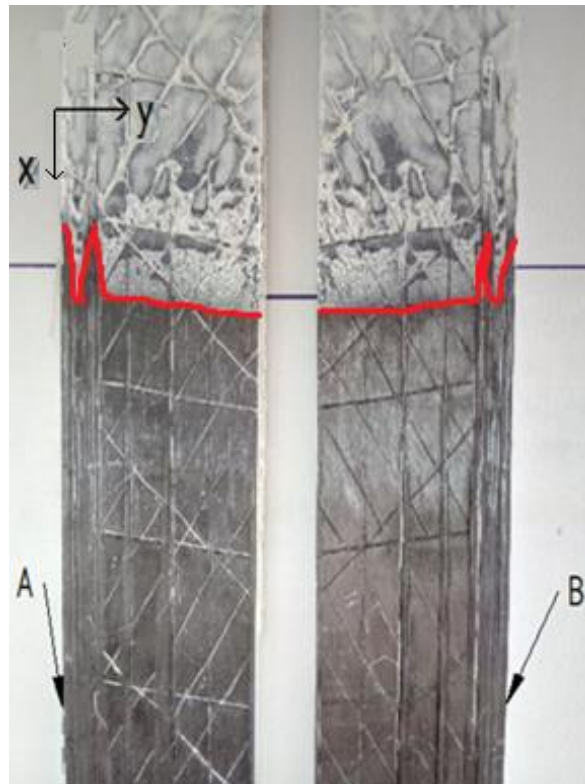


Figure 7. Delamination front in specimen with $0^\circ//30^\circ$ delamination interface after the DCB test.



Figure 8. Delamination front in specimen with $0^\circ//45^\circ$ delamination interface after the DCB test.

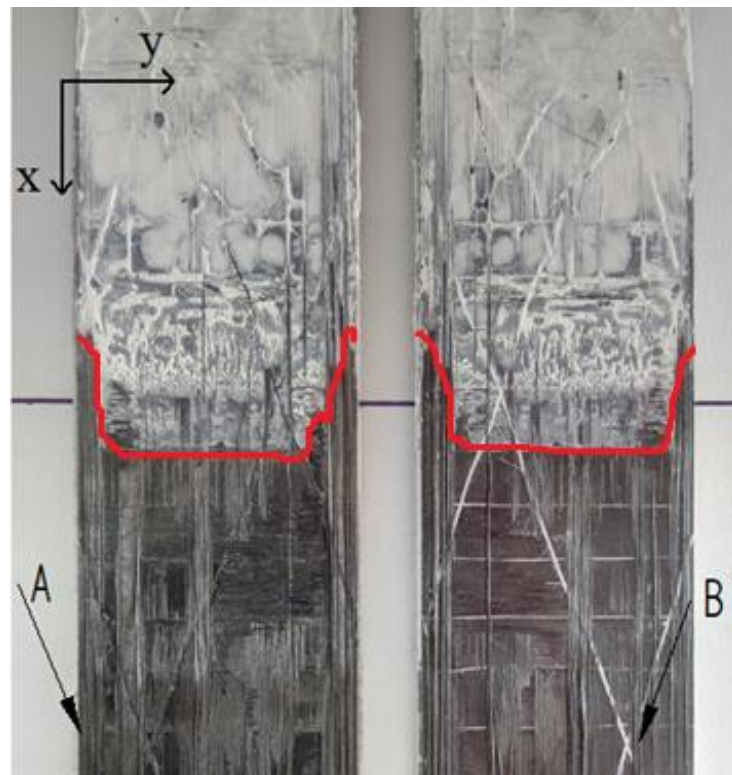


Figure 9. Delamination front in specimen with $0^\circ//90^\circ$ delamination interface after the DCB test.

2.2.5. Analysis of influence of additional θ layers

An additional analysis on the CFRP laminates was performed to investigate the influence of the θ layers on parameters B_{16} and D_{16} , which are responsible for shear strain and twisting curvature under mode I load. The 0°_n layers were replaced by θ_n layers forming new stacking sequences, namely: $[\theta_n/-\theta//\theta/\theta_n]$, $[\theta_n/\theta//\theta/\theta_n]$, $[\theta_n/0^\circ//\theta/\theta_n]$. The influence of the number of θ layers on the values of B_{16} and D_{16} is presented in figures 10, 11, 12, and 13. The analysis reveals that with increased the number of an additional layers in the laminates with interfaces $-\theta//\theta$, $\theta//\theta$ and $0//\theta$ the non-dimensional components reached significantly greater values for example the value of B_{16} term for the laminate with sequence $[-30^\circ_4/-30^\circ//30^\circ/30^\circ_4]$ was about 10000 MPa*mm² where for the laminate with sequence $[-30^\circ_8/-30^\circ//30^\circ/30^\circ_8]$ increased up to around 40000 MPa*mm². Application of identical fiber orientation angle θ in all layers amplifies the undesirable coupling phenomena in laminates which makes difficulties in proper experimental determination of the energy release rate.

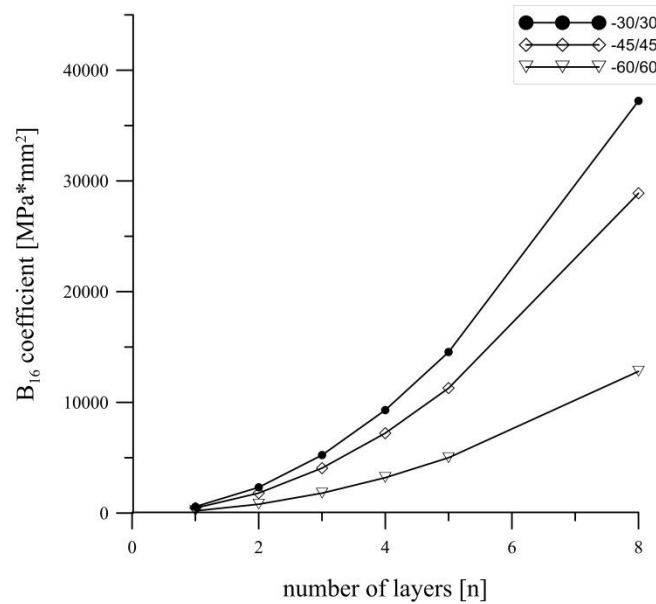


Figure 10. Influence of $[\theta]_n$ layers in laminate with stacking sequence $[\theta_n/-\theta//\theta/\theta_n]$ on the B_{16} component

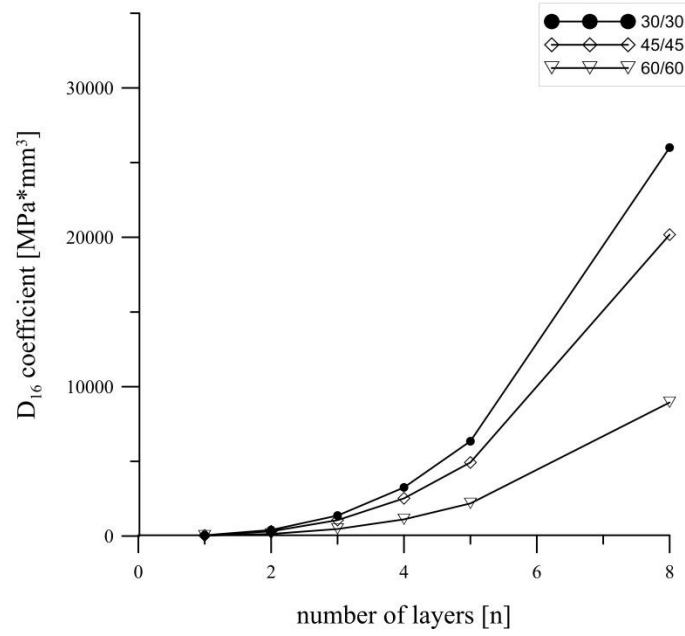


Figure 11. Influence of $[\theta]_n$ layers in laminate with stacking sequence $[\theta_n/\theta//\theta/\theta_n]$ on the D_{16} component

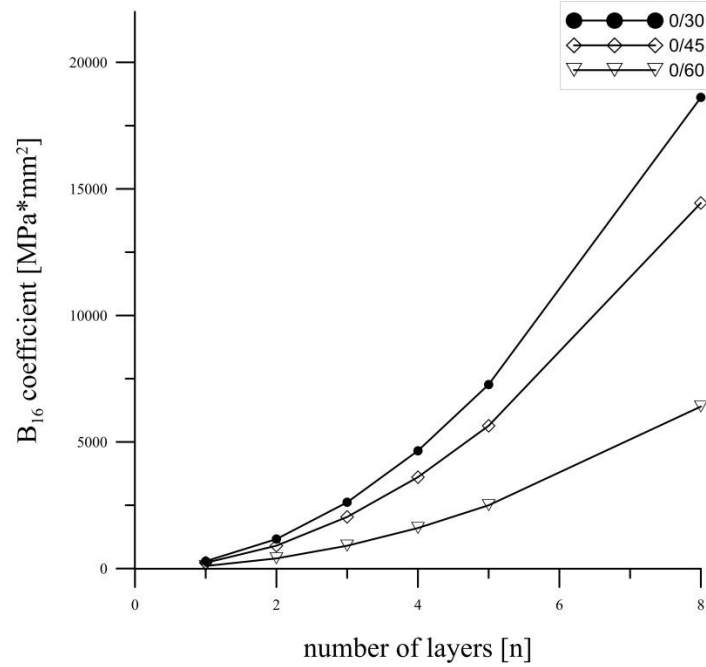


Figure 12. Influence of $[\theta]_n$ layers in laminate with stacking sequence $[\theta_n/0//\theta/\theta_n]$ on the B_{16} component

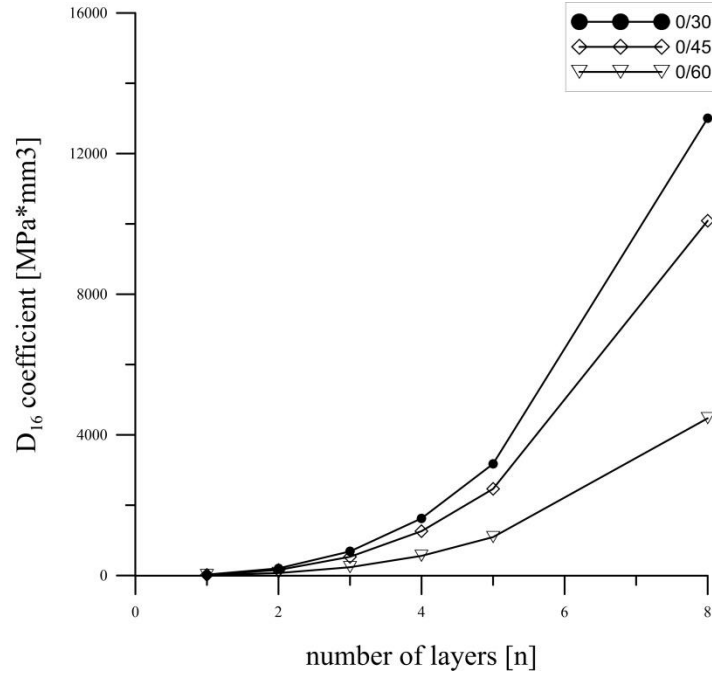


Figure 13. Influence of $[\theta]_n$ layers in laminate with stacking sequence $[\theta_n/0//\theta/\theta_n]$ on the D_{16} component

3. Conclusions

This paper presented analytical study of elastic couplings and a subsequent fractographic analysis of delamination front of carbon/epoxy specimens with different delamination interfaces subjected to DCB tests. Analysis of laminate behavior associated with elastic couplings was performed according to the classical laminate theory. Specimens with interfaces $\theta//-\theta$ exhibited only shear deformation at mid-plane whereas twisting curvature did not exist ($D_{16}=0$) which caused that B_1 parameter was equal to zero. For $\theta//\theta$ interfaces all terms in matrix \mathbf{B} were equal to zero, but non-zero D_{16} component made specimen rotate around longitudinal center axis under bending load. Specimens with delamination interface $0^\circ//\theta$ were fully coupled which caused presence of both shearing deformation and twisting curvature.

Fractographic analysis showed that the effect of elastic couplings in laminates influenced the shape of delamination front in the DCB specimens. In most cases delamination front was strongly

non-uniform and skewed. Moreover, precise determination of crack tip at specimen edges was difficult and visually observed crack tip was not always corresponding to the real crack extent. In any case, the ASTM Standard recommends observation of crack length only at one edge of the specimen. Application of the standardized method to laminates exhibiting elastic couplings may generate errors in experimental measurements of fracture toughness. Therefore, visual observation of crack tip should be conducted on both edges of the specimen.

Additional analysis of influence of the number of θ layers on the B_{16} and the D_{16} components of the coupling stiffness and the bending stiffness matrices showed, that greater number of the same layers strongly amplifies undesirable coupling phenomena which caused shearing and twisting effects, made the delamination front non-uniform and, consequently, it might introduce inaccuracies in the interpretation of the experimental results.

References

- [1] Syafiqah Nur Azrie Safri, Mohamed Thariq Hameed Sultan, Mohammad Jawaaid, Kandasamy Jayakrishna. Impact behaviour of hybrid composites for structural applications: A review. *Composites Part B: Engineering* 2018;133:112–21.
- [2] Ramesh Talreja, Chandra Veer Singh. *Damage and Failure of Composite Materials*. Cambridge University Press; 2012.
- [3] ASTM D5528: Standard Test Method for Mode I Interlaminar Fracture Toughness of Unidirectional Fiber Reinforced Polymer Matrix Composites.
- [4] ASTM D7905: Standard Test Method for Determination of the Mode II Interlaminar Fracture Toughness of Unidirectional Fiber-Reinforced Polymer Matrix Composites.
- [5] ISO 15114: Fibre-Reinforced Plastic Composites - Determination of the Mode II Fracture Resistance for Unidirectionally Reinforced Materials Using the Calibrated End-Loaded Splint (C-ELS) Test and an Effective Crack Length Approach.
- [6] L.A. Carlsson, D.F. Adams, R.B. Pipes. *Experimental characterization of advanced composite materials*, 4th edition. CRC Press; 2014.
- [7] Robert M. Jones. *Mechanics Of Composite Materials*, 2nd Edition. Taylor & Francis; 1999.

- [8] Paolo S. Valvo. On the calculation of energy release rate and mode mixity in delaminated laminated beams. *Engineering Fracture Mechanics* 2016;165:114–39.
- [9] J.W. Hutchinson, Z. Suo. Mixed mode cracking in layered materials. *Advances in Applied Mechanics* 1991;29:63–191.
- [10] A. B. Pereira, A. B. de Morais, M. F. S. F. de Moura, A. G. Magalhães. Mode I interlaminar fracture of woven glass/epoxy multidirectional laminates. *Composites Part A: Applied Science and Manufacturing* 2005;36(8):1119–27.
- [11] A.B. de Morais, M.F. de Moura, A.T. Marques, P.T. de Castro. Mode-I interlaminar fracture of carbon/epoxy cross-ply composites. *Composites Science and Technology* 2002;62:679–86.
- [12] S. Bennati, M. Colleluori, D. Corigliano, P.S. Valvo. An enhanced beam-theory model of the asymmetric double cantilever beam (ADCB) test for composite laminates. *Composites Science and Technology* 2019;69:1735–45.
- [13] A. B. Pereira, A. B. de Morais, A. T. Marques, P. T. de Castro. Mode II interlaminar fracture of carbon/epoxy multidirectional laminates. *Composites Science and Technology* 2004;64(10-11):1653–9.
- [14] N.S. Choi, A. J. Kinloch, J. G. Williams. Delamination fracture of multidirectional carbon–fiber/epoxy composites under mode I, mode II and mixed-mode I/II loading. *Journal of Composite Materials* 1999;33:73–100.
- [15] A. Laksimi, A. Ahmed Benyahia, M.L. Benzeggagh, X.L. Gong. Initiation and bifurcation mechanisms of cracks in multi-directional laminates. *Composites Science and Technology* 2000(60):597–604.
- [16] X.J. Gong, A. Hurez, G. Verchery. On the determination of delamination toughness by using multidirectional DCB specimens. *Polymer Testing* 2010;29:685–666.
- [17] Christopher Bronn York, Sérgio Frascino Müller de Almeida. On Extension-Shearing Bending-Twisting coupled laminates. *Composite Structures* 2017;164:10–22.
- [18] Daokui Li, Christopher B. York. Bounds on the natural frequencies of laminated rectangular plates with extension-twisting (and shearing–bending) coupling. *Composite Structures* 2015;131:37–46.
- [19] Christopher Bronn York, Sergio Frascino Muller de Almeida. Effect of bending-twisting coupling on the compression and shear buckling strength of infinitely long plates. *Composite Structures* 2018;184:18–29.

- [20] S.Samborski. Numerical analysis of the DCB test configuration applicability to mechanically coupled Fiber Reinforced Laminated Composite beams. *Composite Structures* 2016;152:477–87.
- [21] S.Samborski. Analysis of the end-notched flexure test configuration applicability for mechanically coupled fiber reinforced composite laminates. *Composite Structures* 2017;163:342–9.
- [22] J Andersons, M. König. Dependence of fracture toughness of composite laminates on interface ply orientations and delamination growth direction. *Composites Science and Technology* 2004;64(13-14):2139–52.
- [23] Barry D Davidson, R. Krueger, M. Koenig. Three dimensional analysis and resulting design recommendations for unidirectional and multidirectional end-notched flexure tests. *Journal of Composite Materials* 1995;29:2108–33.
- [24] A. B de Morais, M. F de Moura, J. P. M Gonçalves, P. P Camanho. Analysis of crack propagation in double cantilever beam tests of multidirectional laminates. *Mechanics of Materials* 2003;35(7):641–52.

Appendix A – Classical laminate theory

The classical theory of laminate uses a first-order scheme for the strains. Next, the theory makes an additional assumption that consist of neglecting the transverse shear effects. The resultant forces acting at the mid-plane of the laminate, are obtained by integrating the corresponding stress through the laminate thickness h . Similarly, the resultant moments are obtained by integrating the corresponding stress times the moment arm to the mid-plane through the thickness of laminate. As the number of layers in laminate is a finite one, the force-moment system acting at the mid-plane of the laminate can be obtained by replacing the continuous integral by the summation of integrals of each lamina. Therefore,

$$\begin{Bmatrix} N_x \\ N_y \\ N_{xy} \end{Bmatrix} = \int_{-h/2}^{h/2} \begin{Bmatrix} \sigma_x \\ \sigma_y \\ \tau_{xy} \end{Bmatrix} dz = \sum_{k=1}^n \int_{z_{k-1}}^{z_k} \begin{Bmatrix} \sigma_x \\ \sigma_y \\ \tau_{xy} \end{Bmatrix} dz \quad (6)$$

$$\begin{Bmatrix} M_x \\ M_y \\ M_{xy} \end{Bmatrix} = \int_{-h/2}^{h/2} \begin{Bmatrix} \sigma_x \\ \sigma_y \\ \tau_{xy} \end{Bmatrix} z dz = \sum_{k=1}^n \int_{z_{k-1}}^{z_k} \begin{Bmatrix} \sigma_x \\ \sigma_y \\ \tau_{xy} \end{Bmatrix} z dz \quad (7)$$

where: k and n are the current and the total number of plies and z_k is a distance from the laminate mid-plane to the top of the k th ply. Introducing the stress-strain relation for an arbitrary layer given by,

$$\begin{Bmatrix} \sigma_x \\ \sigma_y \\ \sigma_{xy} \end{Bmatrix} = \begin{bmatrix} \bar{Q}_{11} & \bar{Q}_{12} & \bar{Q}_{16} \\ \bar{Q}_{21} & \bar{Q}_{22} & \bar{Q}_{26} \\ \bar{Q}_{16} & \bar{Q}_{26} & \bar{Q}_{66} \end{bmatrix} \begin{Bmatrix} \varepsilon_x \\ \varepsilon_y \\ \gamma_{xy} \end{Bmatrix} = [\bar{Q}_{ij}] \{ \{ \varepsilon_0 \} + z \{ \kappa \} \} \quad (8)$$

where: \bar{Q}_{ij} stands for the transformed reduced stiffness matrix, the ε (or γ) and κ are the strain and curvature components respectively, refers to the neutral plane, the equation for resultant force become,

$$\begin{Bmatrix} N_x \\ N_y \\ N_{xy} \end{Bmatrix} = \sum_{k=1}^n \int_{z_{k-1}}^{z_k} [\bar{Q}_{ij}] k \{ \{ \varepsilon_0 \} + z \{ \kappa \} \} dz \quad (9)$$

$$\{ N \} = \sum_{k=1}^n [\bar{Q}_{ij}] k [z_k - z_{k-1}] \{ \varepsilon_0 \} + \frac{1}{2} \sum_{k=1}^n [\bar{Q}_{ij}] k [z_k^2 - z_{k-1}^2] \{ \kappa \} \quad (10)$$

$$\{ N \} = [A] \{ \varepsilon_0 \} + [B] \{ \kappa \} \quad (11)$$

Similarly, the resultant moment is defined as follows:

$$\begin{Bmatrix} M_x \\ M_y \\ M_{xy} \end{Bmatrix} = \sum_{k=1}^n \int_{z_{k-1}}^{z_k} [\bar{Q}_{ij}] k \{ \{ \varepsilon_0 \} + z \{ \kappa \} \} z dz \quad (12)$$

$$\begin{Bmatrix} M_x \\ M_y \\ M_{xy} \end{Bmatrix} = \sum_{k=1}^n \left[\bar{Q}_{ij} \right] k \int_{z_{k-1}}^{z_k} \{ \varepsilon_0 \} z dz + \sum_{k=1}^n \left[\bar{Q}_{ij} \right] k \int_{z_{k-1}}^{z_k} \{ \kappa \} z^2 dz \quad (13)$$

$$\{ M \} = \sum_{k=1}^n \left[\bar{Q}_{ij} \right] k \frac{1}{2} [z_k^2 - z_{k-1}^2] \{ \varepsilon_0 \} + \sum_{k=1}^n \left[\bar{Q}_{ij} \right] k \frac{1}{3} [z_k^3 - z_{k-1}^3] \{ \kappa \} \quad (14)$$

$$\{ M \} = [B] \{ \varepsilon_0 \} + [D] \{ \kappa \} \quad (15)$$

The constitutive equation of laminate expresses the resultants force and moments as function of the in-plane strains and of the curvatures. It is obtained by regrouping expressions eq.(11) and eq. (15) into a single matrix equation which can be expressed in condensed form as follows:

$$\begin{Bmatrix} \mathbf{N} \\ \mathbf{M} \end{Bmatrix} = \begin{bmatrix} \mathbf{A} & \mathbf{B} \\ \mathbf{B} & \mathbf{D} \end{bmatrix} \begin{Bmatrix} \boldsymbol{\varepsilon}^0 \\ \boldsymbol{\kappa}^0 \end{Bmatrix}, \quad (16)$$

The terms of the matrices \mathbf{A} (the extensional stiffness matrix), \mathbf{B} (the coupling stiffness matrix) and \mathbf{D} (the bending stiffness matrix) can also be expressed by introducing the z_k^c being the k -th ply center of gravity location dimension with respect to the laminate mid-plane and t_k – the k -th ply thickness, in the form:

$$A_{ij} = \sum_{k=1}^n [\bar{Q}_{ij}]_k (z_k - z_{k-1}) = \sum_{k=1}^n [\bar{Q}_{ij}]_k t_k = \begin{bmatrix} A_{11} & A_{12} & A_{16} \\ A_{21} & A_{22} & A_{26} \\ A_{16} & A_{26} & A_{66} \end{bmatrix} \quad (17)$$

$$B_{ij} = \frac{1}{2} \sum_{k=1}^n [\bar{Q}_{ij}]_k (z_k^2 - z_{k-1}^2) = \sum_{k=1}^n [\bar{Q}_{ij}]_k t_k z_k^c = \begin{bmatrix} B_{11} & B_{12} & B_{16} \\ B_{21} & B_{22} & B_{26} \\ B_{16} & B_{26} & B_{66} \end{bmatrix} \quad (18)$$

$$D_{ij} = \frac{1}{3} \sum_{k=1}^n [\bar{Q}_{ij}]_k (z_k^3 - z_{k-1}^3) = \sum_{k=1}^n [\bar{Q}_{ij}]_k \left(t_k (z_k^c)^2 + \frac{t_k^3}{12} \right) = \begin{bmatrix} D_{11} & D_{12} & D_{16} \\ D_{21} & D_{22} & D_{26} \\ D_{16} & D_{26} & D_{66} \end{bmatrix} \quad (19)$$

The coupling behavior is dependent on the components of the each of the extensional **A**, coupling **B** and bending **D** stiffness matrices. For instance, B_{16} and B_{26} couple in-plane normal forces to twisting curvatures and twisting moment to mid-plane normal strains. Elsewhere, D_{16} and D_{26} components couple bending moments to twisting curvature and twisting moment to bending curvature. There is existed a number of coupling types between normal forces, shear strains, bending moments or twisting curvatures which can be eliminated by properly constructed laminate.